DOI: 10.1002/chem.200700305

# Supramolecule-Regulated Photophysics of Oligo(*p*-phenyleneethynylene)-Based Rod–Coil Block Copolymers: Effect of Molecular Architecture

**Kan-Yi Pu,[a, b] Xiao-Ying Qi,[b] Yan-Lian Yang,[c] Xiao-Mei Lu,[d] Ting-Cheng Li,[b] Qu-Li Fan,*[a] Chen Wang,[c] Bin Liu,[e] Hardy Sze On Chan,[d] and Wei Huang*[a]**

**Abstract:** Three new topology-varied rod–coil block copolymers, comprising the same oligo(*p*-phenyleneethynylene) (OPE) rod components and the same coil components, were synthesized by atom-transfer radical polymerization. Their photophysical properties were systematically studied and compared in consideration of their solid-state structures and self-assembly abilities. These copolymers have similar intrinsic photophysical properties to the OPE rods, as reflected in dilute solution. However, their photophysical properties in the solid state are manipulated to be dissimilar by supramolecular organization. Wide-angle X-ray diffraction (WAXD) and atomic force microscopy (AFM) data demonstrate that these copolymers possess different self-assembly abilities due to the molecular-architecture-dependent π–π interactions of the rods. Hence, the aggregates in the solid state are formed with a different mechanism for these copolymers, bringing about the discrepancy in the solid-state luminescent properties.

**Keywords:** block copolymers · luminescence · self-assembly

## Introduction

During the past decades, conjugated polymers have been investigated extensively for their applications in optoelectronic devices, such as light-emitting diodes,[1] photovoltaic cells,[2] organic field-effect transistors,[3] and sensors.[4] The performance of optoelectronic devices is determined mainly by the interchain behaviors, rather than by the intrinsic properties of the conjugated polymers.[5] To control and take advantage of their interchain behavior, conjugated polymers or oligomers have been introduced into a rod–coil block copolymer architecture as the rod components.[6] As these emissive rod–coil block copolymers can form a rich variety of nanoscopic organizations, ranging from lamellar, spherical, cylindrical, to vesicular morphologies,[7] it is generally considered that they are providing a new method of constructing supramolecular optoelectronic devices.[8] However, to date, most research has focused on the self-assembly properties of these block copolymers, while their underlying supramolecule-related photophysics is little known.[7,8] In this context, the relationship between the molecular architecture of the rod–coil block copolymer and the supramolecule-regulated photophysical properties of the rod component will be investigated.

Among conjugated polymers, poly(*p*-phenyleneethynylene)s (PPEs) and their derivatives, in which aryl groups are linked by alkyne units, are of considerable interest.[9] One of the most fascinating properties of PPEs is their sensitive chromic behavior upon environmental variation.[10] For instance, when turning from dilute solutions into thin solid films, the absorption and emission spectra of PPEs always have a larger bathochromic shift relative to other conjugated polymers, such as polyfluorenes and poly(phenylene vi-

[a] K.-Y. Pu, Dr. Q.-L. Fan, Prof. W. Huang
Institute of Advanced Materials (IAM)
Nanjing University of Posts and Telecommunications (NUPT)
66 XinMoFan Road, Nanjing 210003 (China)
Fax: (+86) 25-8349-2333
E-mail: iamqlfan@njupt.edu.cn
wei-huang@njupt.edu.cn

[b] K.-Y. Pu, X.-Y. Qi, Dr. T.-C. Li
Institute of Advanced Materials
Fudan University
Shanghai 200433 (China)

[c] Dr. Y.-L. Yang, Prof. C. Wang
National Center for Nanoscience and Technology
Beijing, 100080 (China)

[d] X.-M. Lu, Prof. H. S. O. Chan
Department of Chemistry, National University of Singapore
Singapore 117543 (Singapore)

[e] Prof. B. Liu
Department of Chemical and Biomolecular Engineering
National University of Singapore
Singapore 117576 (Singapore)

Supporting information for this article is available on the WWW under http://www.chemeurj.org/ or from the author.

   

nylene)s.[11–12] In previous studies, the bathochromic shifts of PPEs were attributed either to the aggregate or to the backbone planarization.[9–10] The aggregate is an interchain behavior, which involves intimate π–π interaction of two or more chromophores in the ground state by extending the delocalization of π-electrons over those chromophores.[13] It usually leads to bathochromic shifts or new peaks in the spectra. In contrast, the backbone planarization is an intrachain behavior, which is associated with the conformational transformation of a single chain.[14] The first interpretation of the spectral shifts of PPEs in terms of aryl twisting and planarization was offered by Bunz et al.[15] In actual fact, for most conjugated polymers, when the conformation of a polymer chain changes from a twisted one into a relatively planar one, the π-electron delocalization along the backbone would become easier, and hence the spectra would red-shift to a certain extent.[16] However, it has been found that this intrachain effect is extremely strong for PPEs, owing to the relatively low rotational barrier of the aryl–alkyne single bonds along the backbone, which is estimated at less than 1 kcal mol$^{-1}$.[17] A recent study with 9,10-bis(phenylethynyl)-anthracene as a model compound showed that the planarization and conformational dynamics of the three aryl rings result in drastic changes in the spectra, which are manifested in the formation of the aggregates.[18] On the other hand, the backbone planarization will give rise to a closer interchain contact, which in turn facilitates the formation of the aggregates in most circumstances.[19]

To control the interchain behavior of PPEs, they have been recently incorporated into linear rod–coil block copolymers as the rod components,[20] or grafted by polymers.[21] It was hoped that the π–π interactions in these grafted PPEs would be restrained by the coil segments. Consequently, the solid-state absorption and emission spectra should retain the features seen in dilute solution. In fact, the results were not as expected. When dividing these grafted PPEs into two kinds, as depicted in Scheme 1 based on the

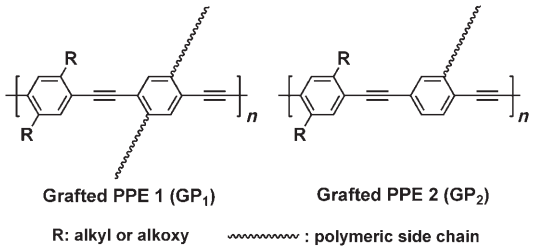


Scheme 1. Schematic representation of the chemical structures of the grafted PPEs.

molecular architecture, it is interesting to find that upon going from dilute solution to thin films, the grafted PPEs with the structure **GP$_1$** (Scheme 1) showed slightly red-shifted absorption and emission spectra,[21a–d] while the grafted PPEs with the structure **GP$_2$** (Scheme 1) exhibited significantly red-shifted and broadened spectra, especially for the emission spectra.[21e–f] However, the photophysical properties of these copolymers were not studied in detail, and satisfactory explanations for these spectral changes were not given in the literature. We envisage that this discrepancy of spectral changes for these grafted PPEs should be ascribed to the different molecular architecture, which plays an important role in determining the intra- and interchain behaviors. Thereby, as aforesaid, it is highly desirable to address the issue of the effect of molecular architecture on the photophysics of emissive block copolymers.

In this contribution, to investigate the effect of molecular architecture on the photophysics of emissive rod–coil block copolymers, we designed and synthesized three new rod–coil block copolymers as model systems containing the same oligo(*p*-phenyleneethynylene) (OPE) chromophores as the rod components and the same coils, but with different molecular architectures as shown in Scheme 2. We will present

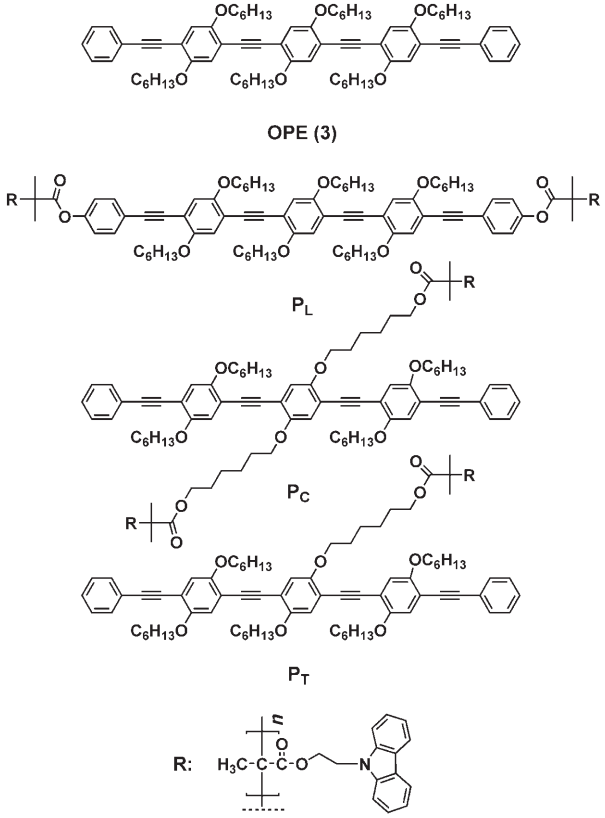


Scheme 2. Chemical structures of the block copolymers and OPE.

the first systematic comparative study on the photophysical properties of OPE and these OPE-based topology-varied block copolymers. OPE was chosen instead of the polymer so that the chemical defects and polydispersities formed during Sonogashira coupling polymerization could be avoided. Atom-transfer radical polymerization (ATRP) was applied to endow these block copolymers with the same coils at different positions on the OPE molecule. Meanwhile, on

  

account of the potential application of these copolymers, poly(2-(carbazol-9-yl)ethyl methacrylate) (PCzEMA), rather than other flexible polymers such as polystyrene and poly(methyl methacrylate), was selected as the coil component, owing to its unique electronic properties as demonstrated in our previous studies.[22] Three rod–coil block copolymers were synthesized: the linear block copolymer ($\mathbf{P_L}$), the cross-shaped block copolymer ($\mathbf{P_C}$), and the T-shaped block copolymer ($\mathbf{P_T}$). Among these copolymers, $\mathbf{P_C}$ and $\mathbf{P_T}$ are the model compounds of $\mathbf{GP_1}$ and $\mathbf{GP_2}$, respectively.

## Results and Discussion

**Synthesis and characterization**: ATRP, as one of the most popular controlled radical polymerizations, provides an effective strategy to construct well-defined polymers with varying composition, functionality, and also architecture, which is difficult or sometimes even impossible for the traditional polymerization technologies.[23] By using a convergent method with a series of well-known organic reactions, such as the Sonogashira coupling reaction and the Williamson ether reaction, the hydroxyl groups were integrated into the different positions of OPE and the macroinitiator precursors (compounds **1**–**8**, see Scheme S1 in the Supporting Information for their structures), with the aim to construct linear, T-shaped, and cross-shaped block copolymers. Such precursors were successfully synthesized in satisfactory yields, shown in Scheme S1 in the Supporting Information as **4**, **7a**, and **7b**, respectively. Meanwhile, the model compound **3**, oligo(2,5-dihexyloxy-1,4-phenyleneethynylene), to be used for comparison, was also prepared by a similar procedure. Finally, these macroinitiator precursors were esterified with 2-bromoisobutyryl bromide to obtain the final OPE macroinitiators, **8a**, **8b**, and **8c**, with high yields close to 100%. The chemical structures of both the precursors and the macroinitiators were confirmed by $^1$H and $^{13}$C NMR spectroscopy. In addition, the macroinitiators and **3** (OPE) were further verified by their matrix-assisted laser desorption ionization-time-of-flight mass spectra (MALDI-TOF MS) (see Figure S1 in the Supporting Information).

In our previous work, we studied ATRP of CzEMA, and well-controlled PCzEMA was gained.[23] In this study, similar ATRP conditions were used to synthesize block copolymers with different molecular architectures, but containing the same components, shown in Scheme 2: $\mathbf{P_L}$, $\mathbf{P_C}$, and $\mathbf{P_T}$. To the best of our knowledge, this is the first report of the synthesis of an OPE-based T-shaped rod–coil diblock copolymer. The degree of polymerization of each coil block of these copolymers was pre-designed to be 20. The ATRP conditions are summarized in Table 1. The polydispersities and molecular weights of these copolymers were determined by gel permeation chromatography (GPC). Figure 1 illustrates the GPC profiles of the copolymers, and also the linear macroinitiator (**8a**) as a representative of the macroinitiators for comparison, indicating that ATRP was performed well upon these macroinitiators and the desired polymer components with low polydispersities were achieved.

Table 1. ATRP conditions and results of the block copolymers.[a]

| Entry | M/S [w/v][b] | $t$ [min] | Conv. [%][c] | $M_n$ (theor)[d] | $M_n$ (NMR) | $M_n$ (GPC)[e] | $M_w/M_n$[e] |
|---|---|---|---|---|---|---|---|
| $\mathbf{P_C}$ | 2:5 | 150 | 93 | 11800 | 10200 | 9800 | 1.16 |
| $\mathbf{P_L}$ | 2:5 | 150 | 92 | 11700 | 10700 | 10400 | 1.18 |
| $\mathbf{P_T}$ | 2:5 | 120 | 94 | 6400 | 6600 | 5500 | 1.14 |

[a] [dNBpy]/[CuCl]/[I] = 4:2:1. All the ATRP reactions were conducted at 90 °C. [b] Ratio of monomer versus solvent [g mL$^{-1}$]. [c] The conversion was determined by comparing the relative integrals of the isolated peaks for monomer and polymer. [d] The theoretical molecular weight was calculated by the conversion rate of monomer and the monomer-initiator ratio. [e] $M_n$ and $M_w/M_n$ were determined by GPC using polystyrene standards.

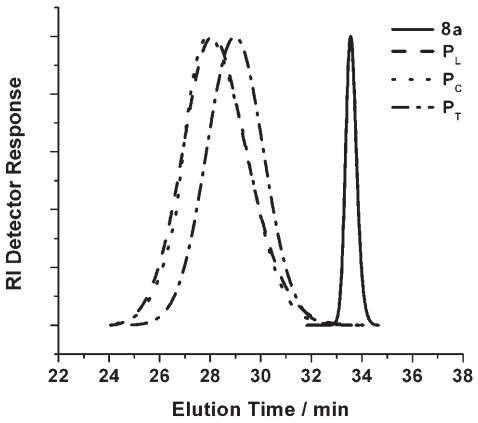


Figure 1. GPC profiles of **8a** and the block copolymers.

The chemical structures of these polymers were determined by $^1$H and $^{13}$C NMR spectroscopy. As a representative example, the $^1$H and $^{13}$C NMR spectra of $\mathbf{P_L}$ coupled with its related macroinitiator (**8a**) are represented in Figures 2 and 3, respectively, which all follow linear superposition of **8a** and PCzEMA. In the $^1$H NMR spectrum of $\mathbf{P_L}$, the existence of the peak at $\delta = 1.84$ ppm due to the alkoxyl

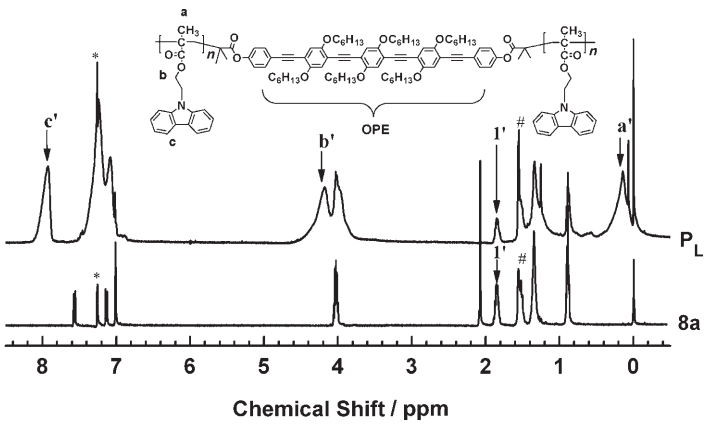


Figure 2. $^1$H NMR spectra of **8a** and the related block copolymer ($\mathbf{P_L}$) in $CDCl_3$. (Symbols * and # represent peaks from $CDCl_3$ and $H_2O$, respectively).

  

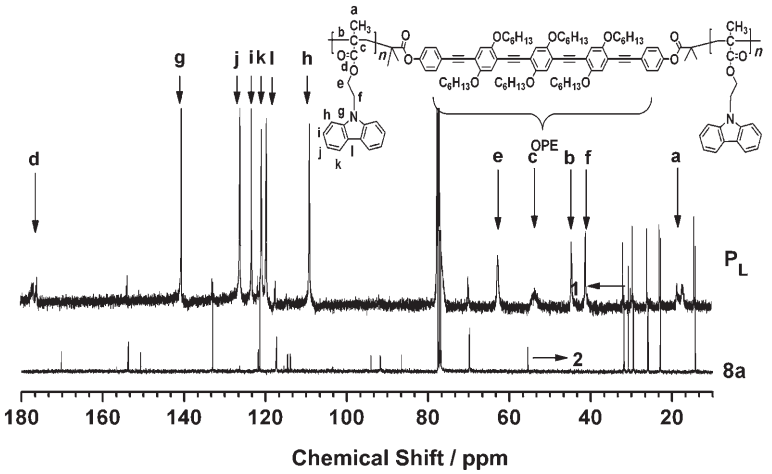


Figure 3. $^{13}$C NMR spectra of **8a** and the related block copolymer ($\mathbf{P_L}$) in $CDCl_3$.

sides of the OPE segment ($-CH_2-$) shows the successful incorporation of OPE into the block copolymer, while the disappearance of the peak at $\delta = 2.08$ ppm due to the resonance of $-C(CH_3)Br$ indicates that **8a** is fully initiated in ATRP. This conclusion could also be drawn from the $^{13}$C NMR spectrum of $\mathbf{P_L}$, that is, the peaks at $\delta = 30.68$ and 55.51 ppm (shown as peaks **1** and **2** in Figure 3), assigned to the $-C(=O)C(\boldsymbol{C}H_3)_2Br$ and $-C(=O)\boldsymbol{C}(CH_3)_2Br$ of **8a**, respectively, are absent in the $^{13}$C NMR spectrum of $\mathbf{P_L}$ due to the local changes in the chemical environment after polymerization. Similar results could be obtained from the $^1$H and $^{13}$C NMR spectra of $\mathbf{P_T}$ and $\mathbf{P_C}$ (see Figure S2 in the Supporting Information). Furthermore, the polymer composition can be estimated according to the ratio between the relative integrals of the isolated peak from the carbazyl proton of the PCzEMA block at $\delta = 7.92$ ppm (shown as peak **c′** in Figure 2) and the isolated peak from the alkyl sides of the OPE segment ($-CH_2-$) at 1.84 ppm (shown as peak **1′** in Figure 2). The results are summarized in Table 1, and are in line with the data from GPC.

**Solid-state structure**: The solid-state photophysical properties of conjugated molecules depend on the solid-state packing structure, rather than being intrinsic properties.[5] Therefore investigating the solid-state structures of these compounds would provide useful information for better understanding their photophysical properties.

The thermal properties of **3**, $\mathbf{P_L}$, $\mathbf{P_T}$, and $\mathbf{P_C}$ were examined by differential scanning calorimetry (DSC) and their thermograms are depicted in Figure 4. The traces of **3** are similar to those reported previously,[24] featuring a melting peak at 118 °C for the second heating scan and a crystallization peak at 103 °C for the first cooling scan. After introduction of PCzEMA as coils, all the copolymers show only a glass-transition temperature at around 125 °C for the second heating scan instead of any melting peaks, which is consistent with the PCzEMA homopolymer.[22]

To further identify the solid-state structures of the copolymers and **3**, wide-angle X-ray diffraction (WAXD) was carried out (Figure 5). These WAXD samples were prepared in the same way as those for the solid-state photophysical studies, so that the connection between the solid-state structures and photophysics could be rationalized. It is known that the solid-state structures of PPEs can, depending on their side-chain type and concentration, display different solid-state supramolecular organization structures, including a cylindrical morphology, a lamellar one, and an interdigitated one.[25] Compound **3** shows a set of clearly resolved reflection peaks, indicating the highly ordered solid-state structure. Among these peaks, the sharp first-order reflection peak at

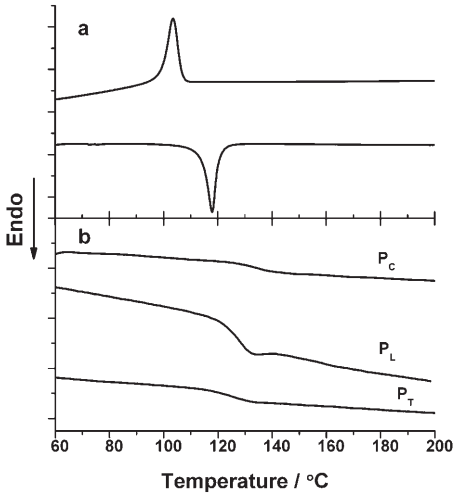


Figure 4. a) DSC profiles of **3**, for the first cooling scan and second heating scan, both at a rate of 10 °C min$^{-1}$. b) DSC profiles of the block copolymers for the second heating scan at a rate of 10 °C min$^{-1}$.

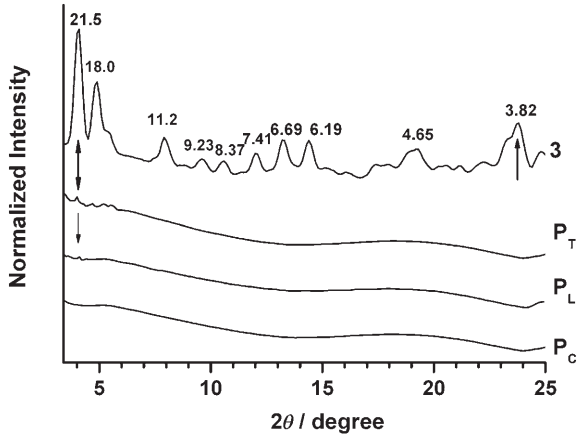


Figure 5. WAXD profiles of **3** and the block copolymers.

  

$2\theta = 4.9°$ corresponding to a *d*-spacing of 18 Å, and the high wide-angle reflection peak at $2\theta = 14.4°$ corresponding to a *d*-spacing of 6.19 Å, are also present in the polymer counterpart of **3**. This has been attributed to the layered packing structure in which the stiff main chains are coplanar.[25a] It is worth noting that the reflection peaks at $2\theta = 23.8°$ corresponding to a *d*-spacing of 3.8 Å stands for the distance between the two parallel packed chains. This short distance usually facilitates the formation of aggregates.[26] In contrast, these OPE-based block copolymers do not show these characteristic reflection peaks of OPE (**3**). However, the reflection peak at 4.1° corresponding to a *d*-spacing of 21.5 Å is weakly visible for $\mathbf{P_T}$ and $\mathbf{P_L}$, which was often observed for the conjugated polymers with hexyloxy side groups.[27] The residue of this peak in $\mathbf{P_T}$ and $\mathbf{P_L}$ reflects the small extent of side chain alignment of the OPE rods. Hence, there should be a few ordered domains in the thin films of $\mathbf{P_T}$ and $\mathbf{P_L}$.[27c–d] However, the invisibility of this peak for $\mathbf{P_C}$ indicates that $\mathbf{P_C}$ is less ordered than $\mathbf{P_T}$ and $\mathbf{P_L}$.

The crystalline property and the layered solid-state packing structure of **3** are evidence of strong π–π interactions, whereas the lack of melting peak and evident characteristic reflection peaks regarding the OPE rods for these copolymers is indicative of the greatly reduced π–π interaction of the rods.

**Solution-state photophysics**: The optical properties of **3** and the macroinitiators in dilute solution are shown in Figure S3 in the Supporting Information. The optical properties of **3** and the macroinitiators in the dilute solutions are nearly identical and in good agreement with their counterparts.[28] For convenience and clarity, **3**, representing all the macroinitiators, will be used for the discussion and comparison of the initiators and their related block copolymers in the following sections.

The optical properties of these copolymers in dilute solutions are shown in Figure 6. In the absorption spectra of the copolymers, two types of absorption bands are present. One ranging from 300 to 350 nm corresponds to the PCzEMA blocks, the other between 350 to around 450 nm is due to the OPE blocks. The absorption spectra also show a compo-

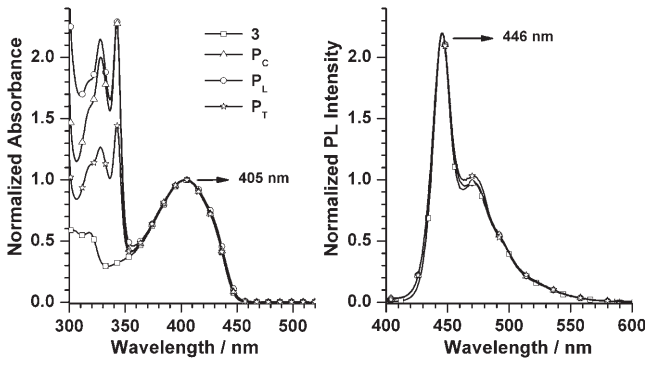


Figure 6. Normalized UV/Vis absorption and PL emission spectra of **3** and the block copolymers in tetrahydrofuran ($10^{-6}$ mg mL$^{-1}$). The excitation wavelength is 405 nm.

nent-dependence similar to our previous study,[22] reflecting that the desired component ratios of these copolymers were achieved. The emission spectra of these copolymers in dilute solution obtained by excitation at 405 nm are nearly identical to that of **3**, exemplifying the maximal emission peaks at 446 nm from the OPE chromophores.

The formation of low-energy sites is usually a diffusion-controlled process. Hence, it is often observed in conjugated oligomers and polymers that owing to the enhanced interchain interactions as well as the occurrence of a sufficient number of collisions at the concentrated solution, low-energy sites including excimers or aggregates are always formed, and this in turn leads to a change of emission spectrum.[29–30] To examine the influence of the solution concentration on the emission spectra of these compounds, the emission spectra with the concentrations of $10^{-6}$ and 1 mg mL$^{-1}$ are shown in Figure 7, all normalized to the maximal emission peak from the OPE chromophores. The emission spectrum of **3** in the concentrated solution changes drastically in contrast to that in dilute solution. The maximal emission peak located at 446 nm in dilute solution is red-shifted by 6 nm to 452 nm in the concentrated solution, indicating the adoption of a planar conformation. Furthermore, the relative intensity at the long-wavelength side increases sharply, which is consistent with the similar OPE compounds in the previous report and could be attributed to the formation of low energy sites.[31] For $\mathbf{P_L}$ and $\mathbf{P_T}$, the maximal emission peak is also red-shifted by 3 nm and 5 nm, respectively, and the relative intensity at the long-wavelength side is slightly increased to a different extent. However, for $\mathbf{P_C}$, the emission band is extremely stable, witnessed by the nearly identical emission bands at these two different concentrations. It is important to point out that the same phenomenon could also be observed from a solution using a different solvent, such as toluene or chloroform. Thus the solvent-induced dissimilarity in photophysical properties is not in-

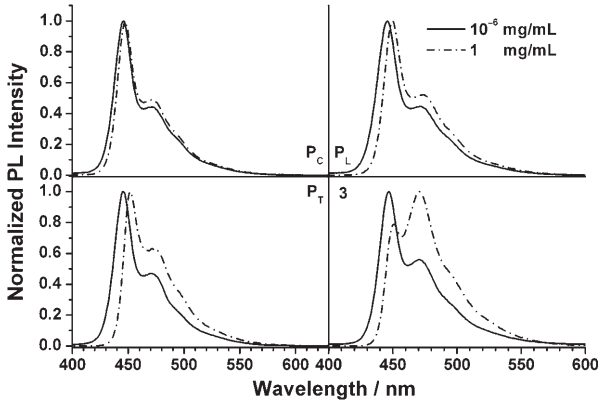


Figure 7. Normalized PL emission spectra of **3** and the block copolymers in dilute and concentrated solutions. The excitation wavelength of the PL emission spectra is 405 nm.

  

volved here, because these compounds have the same good solubility due to the very similar components.[32]

**Solid-state photophysics**: The solid-state absorption and emission spectra of **3** and these copolymers are illustrated in Figure 8. As expected by their solid-state structures, these

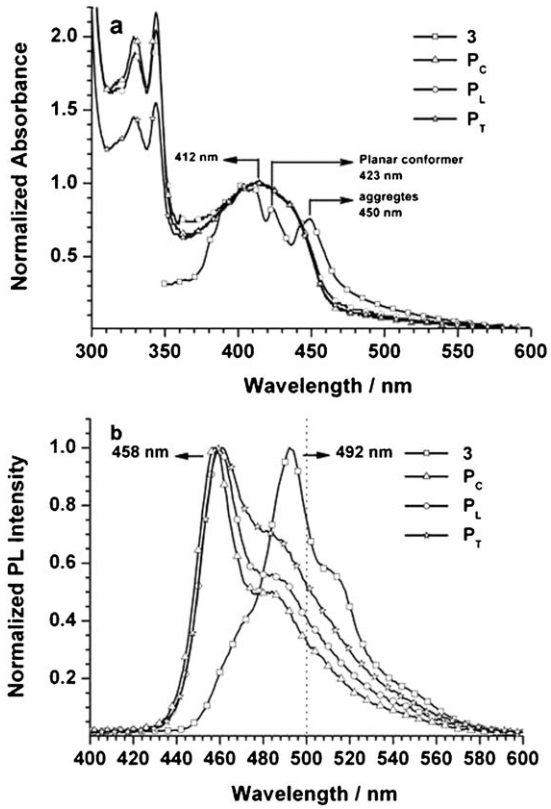


Figure 8. a) Normalized UV/Vis absorption spectra and b) PL emission spectra of **3** and the block copolymers in thin films. The excitation wavelength is 405 nm.

copolymers exhibit clearly different solid-state photophysical properties in contrast to **3**. To probe the origin of this discrepancy, photoluminescence excitation (PLE) and time-resolved photoluminescence (PL) were carried out at the same time.

As for **3**, both the solid-state absorption spectrum and the emission spectrum are largely red-shifted relative to those in the solution state, implying that aggregates may be formed owing to the layered packing structure as detected by WAXD. The solid-state absorption spectrum of **3** is complicated, featuring two adjacent peaks at 412 and 424 nm and also a relatively weak and red-shifted peak at 450 nm (Figure 8). The solid-state emission spectrum of **3** shows a maximal peak located at 492 nm with a 45 nm red-shift compared to the dilute solution state. The PLE spectrum of **3** monitored at 492 nm is different from the absorption spectrum. It shows a maximal peak at 450 nm (Figure 9). This shows that the maximal solid-state emission peak mainly roots from the emission species with the maximal absorption

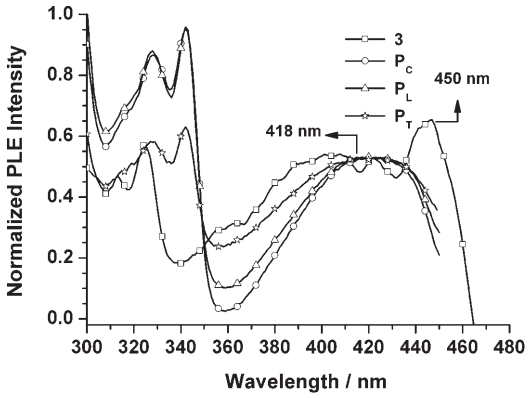


Figure 9. Normalized PLE spectra of **3** and the block copolymers in thin films, monitored at 493 nm and 458 nm, respectively.

peak at around 450 nm. Excimers are dimers of the same chromophores and exist only under excitation, but are dissociative in the ground state. Therefore, the excimers do not have any absorption peak. On the other side, the aggregates are the new ground-state species formed by extending the delocalization of π-electrons over those chromophores. Hence the aggregates have an absorption peak.[13] Thus the emission species with the absorption peak at around 450 nm could result from the aggregates but not from the excimers. Moreover, the decay dynamics of the emission peak at 492 nm is well fitted by a double-exponential with lifetimes of 0.614 ns (28%) and 1.96 ns (72%) (Table 2). This shows

Table 2. Time-resolved PL decay-fitting parameters of **3** and the block copolymers.[a]

| Entry | $\lambda_{probe}$ [nm] | $\tau_1$ [ns][b] | $\tau_2$ [ns][b] | $\chi^2$ |
|---|---|---|---|---|
| **3** | 493 | 0.590 (0.28) | 1.96 (0.72) | 1.085 |
| | 500 | 0.587 (0.20) | 2.24 (0.80) | 1.119 |
| $\mathbf{P_C}$ | 458 | 0.621 (1.00) | | 1.229 |
| | 500 | 0.723 (0.84) | 2.97 (0.16) | 1.051 |
| $\mathbf{P_L}$ | 460 | 0.606 (1.00) | | 1.131 |
| | 500 | 0.714 (0.78) | 2.86 (0.22) | 1.273 |
| $\mathbf{P_T}$ | 461 | 0.599 (1.00) | | 1.056 |
| | 500 | 0.703 (0.65) | 2.94 (0.35) | 1.211 |

[a] Films are excited at 371 nm, thereby, excitation of the PCzEMA blocks of the block copolymers is avoided. [b] Values given in percentages.

that two emission species are responsible for the emission at 492 nm. The double-exponential decay dynamics with the domination of the longer lifetime safely affirms the formation of the aggregates.[33] Consequently, the emission species with the absorption peak at 450 nm could be due to the aggregates. It is known that PPE systems always exhibit significant conformation-dependent photophysical properties, as mentioned in the Introduction section.[14] Thereby, the other absorption peaks at 412 and 424 nm in the solid-state absorption spectrum of **3** could be naturally attributed to the unimolecular OPE with a different extent of backbone planarization.[34] The absence of the emission from the unimo-

  

lecular OPE molecules could be explained by the efficient energy transfer from them to the aggregates in the solid state, in which the energy transfer is an efficient three-dimensional process.[16] The designation of these peaks coincides with the literature in which the aggregation behaviors of oligo(2,5-dibutoxy-1,4-phenyleneethynylene), the analogue of **3** in this study, were studied by Pang et al.[28b]

As for these copolymers, in accordance with the WAXD data, the peak of the aggregates does not show up markedly in the solid-state absorption spectra due to the evident absence of strong π–π interactions (Figure 8). Instead, all these copolymers display two kinds of absorption bands, the band ranging from 300 to 350 nm and the band between 350 to around 460 nm, corresponding to the PCzEMA and the OPE blocks, respectively. In contrast to the dilute solution state, the maximal absorption peaks from the OPE chromophores of these copolymers in the solid state was slightly red-shifted by 8 nm from 404 to 412 nm. On the basis of the assignment of the similar solid-state absorption peak at 412 nm of **3**, the slightly red-shifted absorption bands stem from the unimolecular OPE chromophores adopting planar conformations with respect to the twisted conformations in the dilute solution. In the solid-state emission spectra, all these copolymers show a maximal peak slightly red-shifted by 13 nm relative to that in the solution state (Figure 8). The PLE spectra of these copolymers monitored at this maximal solid-state emission peak are almost identical (Figure 9), showing the broad bands with the maximal peak at around 418 nm almost equal to those of the solid-state absorption spectra. This confirms that the emission at around 458 nm comes from the unimolecular OPE chromophores with the planar conformations rather than from the aggregates. Additionally, time-resolved PL experiments exhibit single-exponential decay dynamics of these maximal emission peaks with a lifetime around 0.6 ns, comparable to around 0.7 ns in the dilute solution (Table 2), which further proves this conclusion. Meanwhile, it is known that in the solution state the rotationally disordered chromophores have to planarize before they emit, while in the solid state the chromophores are already planarized and no significant geometric reorganization between ground and excited state is necessary.[35] Thus, the relatively shorter decay time in the solid state compared to the dilute solution is also indicative of the adoption of the planar conformations. A similar phenomenon is also observed for PPEs.[12b] However, it should be noted that the homogeneous and broad feature of these absorption bands from 350 to around 460 nm implies that the OPE rods of these copolymers exist in the solid state with a variety of conformations, ranging from the less planar one to the more planar one. Also, because the absorption peak of the aggregates is liable to be hidden under the inhomogeneous broadened absorption spectrum,[36] the possibility that the aggregates may exist in a very small amount in these copolymers merits serious consideration, which will be discussed in the next sections.

From these data, one can see that compound **3** and the OPE segments of the copolymers have nearly identical photophysical properties in the dilute solution state, because the similar twisted conformations are assumed at this approximately unimolecular level at which molecules are separated. Upon increasing the solution concentration, intermolecular behavior begins to occur. As a result, the emission bands of these compounds change to the different profiles, insinuating the different extent of the π–π interactions. In the solid state, molecules contact intensively, and the intermolecular behavior is maximized. Introducing OPE into the rod–coil block copolymers greatly destroys the π–π interactions of the OPE rods due to the shielding effect of the coils.[37] Therefore, differing from the aggregate-occupied solid-state spectra of **3**, all the copolymers exhibit the solid-state spectra dominated by the signals from unimolecular OPE chromophores with planar conformations. In addition, it can be confidently concluded that in contrast to the unimolecular OPE with the twisted conformations, the planar conformers of the OPE chromophores exhibit maximal absorption and emission peaks slightly red-shifted by 10–20 nm, while the aggregates of OPE chromophores have their maximal absorption and emission peaks greatly red-shifted by 30–50 nm. This observation is in perfect agreement with the studies of the effects of chromophore planarization and aggregation on photophysics with 1,4-bis(phenylethynyl)benzene and 1,4-bis(2-hydroxy-2-methyl-3-butynyl)-2-fluorobenzene as the model compounds.[17,19]

**Effect of molecular architecture on forming the aggregates**: As illustrated by the WAXD data, a few ordered domains are present in the thin films of $\mathbf{P_L}$ and $\mathbf{P_T}$, inferred from the weakly visible reflection peak at 4.1°. Taking into account the inhomogeneous broadening in the solid-state absorption spectra of these copolymers, the possibility of forming the aggregates of the OPE rods in these small, ordered domains emerges. Apparently, the solid-state emission spectra of these copolymers extend to the long-wavelength side, and overlap the aggregate dominated emission spectrum of **3**, as shown in Figure 8. The relative intensity at 500 nm in the emission spectra (Figure 8), and the absolute quantum yields of these copolymers in these thin films, are calculated and summarized in Table 3. The relative intensities at 500 nm are in the order of $\mathbf{P_C} < \mathbf{P_L} < \mathbf{P_T}$, while the quantum yields are in the reversal sequence. It has been widely observed that forming the aggregates is always concomitant

Table 3. Photophysical data for comparison.

| Entry | $\mathbf{P_C}$ | $\mathbf{P_L}$ | $\mathbf{P_T}$ |
|---|---|---|---|
| intensity ratio[a] | 1.00 | 1.30 | 1.70 |
| relative intensity[b] | 0.33 | 0.41 | 0.51 |
| $\Phi$[c] | 2.70 | 2.10 | 1.40 |

[a] The intensity ratios at 500 nm for the solution concentration of 1 mg mL$^{-1}$ to that of $10^{-6}$ mg mL$^{-1}$ are calculated from the emission spectra of Figure 7. [b] Relative intensity is according to the emission spectra of Figure 8b. [c] The fluorescence quantum yields in thin films relative to **3** assuming 1.00 for comparison were obtained from the same samples used for photophysical measurements.

  

with an increase in relative intensity at the long-wavelength side as well as a decrease in quantum yields,[36b,38] thus one can foresee that not only are the aggregates of the OPE chromophores formed for these copolymers, but also the populations of the aggregates should be different from each other. It is important to point out that the thin films studied here were prepared from the same concentration of solutions of the sample in tetrahydrofuran (10 mg mL$^{-1}$) under the exactly same spin-casting conditions. Furthermore, the same phenomenon could also be observed by the thin films casting from the solutions by using different solvents such as toluene and chloroform.

To further confirm the existence of the aggregates, PLE and time-resolved PL spectra were performed at 500 nm. The PLE spectra of these copolymers monitored at 500 nm show broad bands extending to the long-wavelength side, with the maximal peak near 439 nm (Figure 10), which is

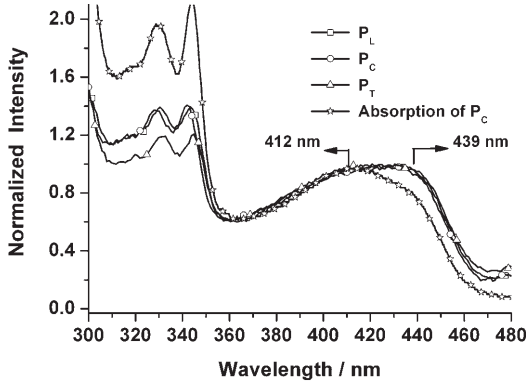


Figure 10. Normalized PLE spectra of the block copolymers in thin films monitored at 500 nm coupled with the absorption spectrum of $\mathbf{P_C}$ for comparison.

different from the PLE spectra monitored at 458 nm with the maximal peak at 418 nm (Figure 9). Relative the absorption spectra, we observe that the maximal peaks are largely red-shifted by around 30 nm, implying that the emission at 500 nm does not come just from the unimolecular species. To further substantiate the point, time-resolved PL experiments were performed upon these copolymers probing at 500 nm, as shown in Figure 11. As expected, all the decays are best described by the double-exponential dynamic mechanism, and the longer lifetime is comparable to that of the aggregates of **3**, attesting that the aggregates are indeed in existence. However, differing from the decay of **3** at 500 nm, all these decays of the copolymers are prevailed by the shorter lifetime species rather than the longer lifetime species of **3**. Considering that there is no evident aggregate peak in the absorption spectra and no reflection peaks at 3.8 nm in WAXD profiles for these copolymers, it is reasonable to believe that although the aggregates are formed, they are in an infinitesimal portion. When comparing the decay dynamics of these copolymers, one finds that the amount ratios of longer life species related to the aggregates

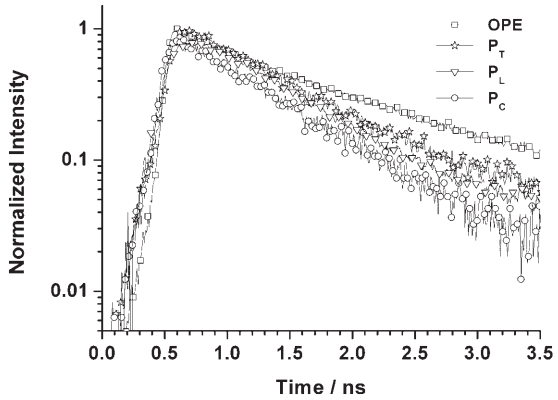


Figure 11. PL decay curves of **3** and the block copolymers in thin films monitored at 500 nm (excitation at 371 nm).

are different from each other with the sequence of $\mathbf{P_C} < \mathbf{P_L} < \mathbf{P_T}$. These different ratios verify that the population of aggregate is different,[33,36] which is the cause of the different relative emission intensities at the long-wavelength side and different quantum yields of the solid state for these copolymers.

In addition, as mentioned in the previous section, when increasing the concentration, the emission spectra of these copolymers turn into different profiles, and the emission intensity at 500 nm increases to a different extent for these copolymers as shown in Figure 7. This implies that aggregates with different amounts for these copolymers are also formed in the concentrated solutions. The ratio of emission intensity at 500 nm for the concentration of 1 mg mL$^{-1}$ to $10^{-6}$ mg mL$^{-1}$ is calculated and summarized in Table 3. These data are in good accordance with the relative emission intensity at 500 nm in the solid state, presenting a gradual increase with the same order of $\mathbf{P_C} < \mathbf{P_L} < \mathbf{P_T}$.

On the basis of this evidence, it can be concluded that the tendency to form the aggregates is different for these copolymers, and determined by the molecular architecture dependent π–π interactions, producing the discrepancy in luminescent properties both in the concentrated solutions and the thin films. The tendency to form the aggregates of the OPE chromophores in these copolymers and **3** follows the order of $\mathbf{P_C} < \mathbf{P_L} < \mathbf{P_T} < \mathbf{3}$.

**Origin of the aggregates**: It is known that the self-assembly ability of a conjugated rod–coil block copolymer is governed not only by the Flory–Huggins interaction and the volume fraction of the two blocks, but also more importantly by the π–π interactions between the rods.[39] As a consequence, concomitant formation of these ordered nanoscopic domains with the appearance of the aggregates is observed.[6a,b,37a,40] Thereby, studying the self-assembly ability of these materials can give a better understanding of the extent of the π–π interactions between the OPE rods, which further helps us understand the origin of the aggregates.

In this respect, tapping-mode atomic force microscopy (AFM) was performed. AFM is known to provide a straight-

  

forward morphological characterization of surfaces with a lateral resolution in the order of a few nanometers, and a vertical resolution in the order of 1 Å.[41] Figure 12 shows

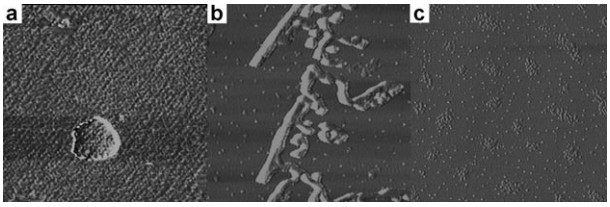


Figure 12. AFM phase images (2×2 μm) of a) $\mathbf{P_T}$, b) $\mathbf{P_L}$, and c) $\mathbf{P_C}$.

the AFM images of these copolymers obtained from the semiconcentrated solutions of the samples in tetrahydrofuran (0.01 mg mL$^{-1}$). The solutions were deposited on a mica substrate in a solvent-saturated atmosphere. These copolymers form different morphologies, which is a reflection of the different self-assembly abilities. Interestingly, $\mathbf{P_T}$ forms a rectangular bilayer packing nanostructure with an average height of 3 nm as shown in Figure 12 a. Glotzer et al. recently reported the simulation of the self-assembly of a T-shaped rod–coil block copolymer. They demonstrated that a rectangular bilayer packing structure of the ribbons rather than a hexagonal packing structure is most favorable for this copolymer due to the competition between maximizing the rod–rod interaction and the entropy contributed by the coils.[42] Thereby, the very similar nanostructure for $\mathbf{P_T}$ reflects that the π–π interactions of the OPE rods are still in existence and play an important role in the self-assembly into this extremely ordered nanostructure. The $\mathbf{P_L}$ copolymer exhibits a typical nanoribbon structure of a linear rod–coil block copolymer, with an average width and height of 100 and 20 nm, respectively (Figure 12b).[43] A similar nanoribbon structure was also observed for PPE-based linear rod–coil block copolymers reported by Lazzaroni's group, which was indicative of the present π stacking of the rod as one of the important driving forces.[44] However, $\mathbf{P_C}$ only shows nanoscale grains with an average diameter and height of 25 and 4 nm, respectively (Figure 12c). This confirms that stemming from the shielding of coils at both sides of the OPE rods, the π–π stacking of the OPE rods of $\mathbf{P_C}$ are further destroyed with respect to $\mathbf{P_T}$ and $\mathbf{P_L}$, which in turn gives $\mathbf{P_C}$ a relatively poor self-assembly ability and low susceptibility to form aggregates. The poorer self-assembling ability of $\mathbf{P_C}$ relative to $\mathbf{P_T}$ and $\mathbf{P_L}$ can also be seen from the WAXD data as shown in the previous section, that is, the reflection peak at 4.1° is absent for $\mathbf{P_C}$ but present for $\mathbf{P_T}$ and $\mathbf{P_L}$.

These results manifest that the π–π interaction of the OPE rods for these copolymers, resulting in these nanostructures, are different and are modulated by the molecular architecture. Besides, the resulting different self-assembly abilities of these copolymers are consistent with the tendency to form aggregates, as deduced from the photophysical studies. Consequently, it further confirms the conclusion that the tendency to form aggregates of the OPE rods in these copolymers follows the order of $\mathbf{P_C} < \mathbf{P_L} < \mathbf{P_T}$. Moreover, one can conclude that the residue of ordered nanostructures in the thin films, in which the π–π interactions of the OPE rods are present, is the possible origin of the formation of the aggregates for these copolymers.

## Conclusion

In summary, we have demonstrated a facile synthetic way to desirably control the molecular architecture of a conjugated rod–coil block copolymer through ATRP. To this end, three new rod–coil block copolymers, consisting of the same OPE as rod components and the same PCzEMA as the coil components, but with different molecular architectures, were prepared. The underlying supramolecule-regulated photophysics of these block copolymers and OPE were systematically studied in detail by combining the spectroscopic, solid-state structural, and self-assembly analyses. The solid-state structures of these compounds were examined by DSC and WAXD. The results illustrate that OPE has a crystalline, ordered packing structure with strong π–π interactions, whereas the copolymers are nearly amorphous, with greatly reduced π–π interactions, especially for $\mathbf{P_C}$. In dilute solution, the copolymers and OPE have almost identical absorption and emission spectra to the OPE chromophores, verifying the similar intrinsic photophysical properties. In the solid state, the absorption and emission spectra of OPE are dominated by the aggregates, while the maximal absorption and emission peaks of the copolymers are dominated by the unimolecular OPE chromophores with planar conformations, in contrast to those in the dilute solution. These observations are consistent with the conclusion drawn from the solid-state structures.

More importantly, the effect of molecular architecture on the photophysical properties of emissive rod–coil block copolymers has been revealed for the first time. As confirmed by AFM and WAXD, these copolymers have dissimilar π–π interactions of the OPE rods, dependent on the molecular architecture, leading to the discrepant tendencies toward aggregates. Thereby, these copolymers have different solid-state emission spectra and quantum yields. Among three block copolymers, the block copolymer with the cross-shaped molecular architecture ($\mathbf{P_C}$), which is the model compound of $\mathbf{GP_1}$, has the weakest π–π interactions of the OPE rods and thereby prevents most strongly the formation of aggregates. The block copolymer with the T-shaped molecular architecture ($\mathbf{P_T}$), which is the model compound of $\mathbf{GP_2}$, is the most susceptible towards aggregates with the strongest π–π interactions and self-assembly ability. On the basis of these data, the different spectral changes of the aforementioned PPE-based graft copolymers upon going from dilute solutions into thin solid films can be attributed to the discrepant tendency to form aggregates. These findings provide profound guidelines for engineering supramolecular opto-

  

electronic devices based on emissive rod–coil block copolymers.

## Experimental Section

**Characterization**: NMR spectra were collected on a Varian Mercury Plus 400 spectrometer with tetramethylsilane as the internal standard. MALDI experiments were carried out using a Shimadzu AXIMA-CFRTM plus time-of-flight mass spectrometer (Kratos Analytical, Manchester, U.K.). The instrument was equipped with a nitrogen laser emitting at 377 nm, a 2 GHz sampling rate digitizer, a pulsed ion extraction source, and an electrostatic reflectron. Spectra were acquired in the positive-ion mode using the reflectron. Elemental analyses were performed on a Vario EL III O-Element Analyzer system. GPC analysis was conducted with a HP1100 HPLC system equipped with 7911GP-502 and GP NXC columns by using polystyrene as the standard and THF as the eluent at a flow rate of 1.0 mL min$^{-1}$ at 35 °C. DSC measurements were performed under a nitrogen atmosphere at heating and cooling rates both of 10 °C min$^{-1}$, with NETZSCH DSC 200PC apparatus. WAXD data was obtained on a Bruker D8 Discover diffractometer with GADDS as a 2D detector. Calibration was conducted using silicon powder and silver behenate. AFM experiments were performed under ambient conditions and room temperature on a Nanoscope IIIa microscope (Digital Instruments, Santa Barbara, CA) operating in a tapping-mode. UV/Vis spectra were recorded on a Shimadzu 3150 PC spectrophotometer. Fluorescence measurements were carried out on a Shimadzu RF-5301 PC spectrofluorophotometer with a xenon lamp as the light source. Time-correlated single photon fluorescence studies were performed using an Edinburgh Instruments LifeSpec-PS spectrometer. The LifeSpec-PS comprises a 371 nm picosecond laser (PicoQuant PDL 800B) operated at 2.5 MHz and a Peltier cooled Hammamatsu microchannel plate photomultiplier (R3809U-50). Lifetimes were determined from the data by using the Edinburgh Instruments software package. Measurement of the absolute PL efficiency was performed on LabsphereIS-080(8″), which contained an integrating sphere coated on the inside with a reflecting material barium sulfate, and the diameter of the integrating sphere was 20.3 cm. PL efficiency was calculated from the software attached by LabsphereIS-080-(8″), and normalized to OPE (**3**) assumed to be 1.00 for facile comparison. The polymer thin films used for the photophysical measurements and WAXD were all prepared by spin-coating from solution of the samples in tetrahydrofuran (10 mg mL$^{-1}$) onto quartz plates at 2500 rpm. The thickness of the films was about 100 nm.

**Materials**: All chemical reagents were purchased from Aldrich Chemical Co. THF was purified by distillation from sodium in the presence benzophenone. Anisole was distilled from calcium hydride and stored under argon in darkness at 0 °C. Copper(I) bromide (CuBr) was purified according to the standard procedure.[45] 1,4-Dihexyloxybenzene,[24] 1,4-dihexyloxy-2,5-diiodobenzene,[24] 1,4-diethynyl-2,5-bis(hexyloxy)benzene,[24] 2-(4-ethynylphenoxy)-tetrahydro-2*H*-pyran,[46] 1,4-diiodo-2,5-hydroquinone,[47] 2-(carbazol-9-yl)ethyl methacrylate (CzEMA),[22] and poly[2-(carbazol-9-yl)ethyl methacrylate] (PCzEMA)[22] were synthesized according to the literature. The detailed synthesis and characterization procedures of the macroinitiators and OPE are given in the Supporting Information.

**ATRP synthesis of block copolymers**: The block copolymers were synthesized by solution polymerization in anisole. In a typical run, a Schlenk tube was charged with macroinitiator (18.0 μmol), 4,4′-dinonyl-2,2′-dipyridyl (dNBipy) (29.4 mg, 72.0 μmol), CzEMA (200 mg, 716 μmol), and CuBr (5.16 mg, 36.0 μmol) before it was sealed with a rubber septum. The Schlenk tube was degassed with three vacuum–argon cycles to remove air and moisture, and then anisole (500 μL) was added to the Schlenk tube. The mixture was frozen, evacuated, and thawed three times to further remove air. The Schlenk tube was immersed in an oil bath at 90 °C to carry out the polymerization. After a period of time, the reaction mixture was cooled in liquid $N_2$ in order to quench the polymerization and diluted with THF, then passed through a column of neutral alumina to remove the catalysts. The polymers were precipitated into an excess of methanol and dried in vacuum at 40 °C. Light or primrose yellow powdery products were obtained.

## Acknowledgements

This work was financially supported by the National Natural Science Foundation of China under Grants 60325412, 90406021, 20504007, 50428303, and NY207011. K.Y.P. also thanks Prof. Chi-Fei Wu, School of Materials Science and Engineering, East China University of Science and Technology, for DSC experiments.

[1] R. H Friend, R. W. Gymer, A. B. Holmes, J. H. Burroughes, R. N. Marks, C. Taliani, D. D. C. Bradley, S. D. A. Dos, J. L. Brédas, M. Lögdlund, W. R. Salaneck, *Nature* **1999**, *397*, 121–128.
[2] G. Yu, J. Gao, J. C. Hummelen, F. Wudl, A. J. Heeger, *Science* **1995**, *270*, 1789–1791.
[3] H. Sirringhaus, N. Tessler, R. H. Friend, *Science* **1998**, *280*, 1741–1744.
[4] L. Chen, D. W. McBranch, H. Wang, R. Helgeson, F. Wudl, D. G. Whitten, *Proc. Natl. Acad. Sci. USA* **1999**, *96*, 12287.
[5] a) C. L. Donley, J. Zaumseil, J. W. Andreasen, M. M. Nielsen, H. Sirringhaus, R. H. Friend, J.-S. Kim, *J. Am. Chem. Soc.* **2005**, *127*, 12890–12899; b) M. Muccini, M. Murgia, F. Biscarini, C. Taliani, *Adv. Mater.* **2001**, *13*, 355–358; c) S. H. Chen, A. C. Su, C. H. Su, S. A. Chen, *J. Phys. Chem. B* **2006**, *110*, 4007–4013; d) W.-Y. Sun, S.-C. Yang, J. D. White, J.-H. Hsu, K.-Y. Peng, S. A. Chen, W. Fann, *Macromolecules* **2005**, *38*, 2966–2973.
[6] a) S. A. Jenekhe, X. L. Chen, *Science* **1998**, *279*, 1903–1907; b) S. A. Jenekhe, X. L. Chen, *Science* **1999**, *283*, 372–375; c) M. A. Hempenius, B. M. W. Langeveld-Voss, J. A. E. H. V. Haare, R. A. J. Janssen, S. S. Sheiko, J. P. Spartz, M. Möller, E. W. Meijer, *J. Am. Chem. Soc.* **1998**, *120*, 2798–2804; d) H. Wang, H. H. Wang, V. S. Urban, K. C. Littrell, P. Thiyagarajan, L. Yu, *J. Am. Chem. Soc.* **2000**, *122*, 6855–6861.
[7] M. Lee, B. K. Cho, W. C. Zin, *Chem. Rev.* **2001**, *101*, 3869–3892.
[8] a) F. J. M. Hoeben, P. Jonkheijm, E. W. Meijer, A. P. H. J. Schenning, *Chem. Rev.* **2005**, *105*, 1491–1546; b) A. P. H. J. Schenning, E. W. Meijer, *Chem. Commun.* **2005**, 3245–3258.
[9] a) U. H. F. Bunz, *Adv. Polym. Sci.* **2005**, *177*, 1–51; b) K. Y. Pu, B. Zhang, Z. Ma, P. Wang, X. Y. Qi, R. F. Chen, L. H. Wang, Q. L. Fan, W. Huang, *Polymer* **2006**, *47*, 1970–1978.
[10] a) U. H. F. Bunz, *Chem. Rev.* **2000**, *100*, 1605–1644; I. Kim, B. Erdogan, J. N. Wilson, U. H. F. Bunz, *Chem. Eur. J.* **2004**, *10*, 6247–6254.
[11] L. Akcelrud, *Prog. Polym. Sci.* **2003**, *28*, 875–962.
[12] a) N. Lebouch, S. Garreau, G. Louarn, M. Belletê, G. Durocher, M. Leclerc, *Macromolecules* **2005**, *38*, 9631–9637; b) U. H. F. Bunz, J. M. Imhof, R. K. Bly, C. G. Bangcuyo, L. Rozanski, D. A. V. Bout, *Macromolecules* **2005**, *38*, 5892–5896.
[13] a) S. A. Jenekhe, J. A. Osaheni, *Science* **1994**, *265*, 765–768; b) Y. Kim, J. Bouffard, S. E. Kooi, T. M. Swager, *J. Am. Chem. Soc.* **2005**, *127*, 13726–13731; c) E. D. Como, M. A. Loi, M. Murgia, R. Zamboni, M. Muccini, *J. Am. Chem. Soc.* **2006**, *128*, 4277–4281.
[14] a) A. Beeby, K. Findlay, P. J. Low, T. B. Marder, *J. Am. Chem. Soc.* **2002**, *124*, 8280–8284; b) P. V. James, P. K. Sudeep, C. H. Suresh, K. G. Thomas, *J. Phys. Chem. A* **2006**, *110*, 4329–4337; c) L. T. Liu, D. Yaron, M. I. Sluch, M. A. Berg, *J. Phys. Chem. B* **2006**, *110*, 18844–18852.
[15] T. Miteva, L. Palmer, L. Kloppenburg, D. Neher, U. H. F. Bunz, *Macromolecules* **2000**, *33*, 652–654.
[16] a) B. J. Schwartz, *Annu. Rev. Phys. Chem.* **2003**, *54*, 141–172; b) S. S. Zade, M. Bendikov, *Chem. Eur. J.* **2007**, *13*, 3688–3700.
[17] a) M. Levitus, K. Schmieder, H. Ricks, K. D. Shimizu, U. H. F. Bunz, M. A. G. Garibay, *J. Am. Chem. Soc.* **2001**, *123*, 4259–4265; b) M. Levitus, K. Schmieder, H. Ricks, K. D. Shimizu, U. H. F. Bunz, M. A. G. Garibay, *J. Am. Chem. Soc.* **2002**, *124*, 8181–8181.

  

[18] M. Levitus, M. A. Garcia-Garibay, *J. Phys. Chem. B* **2000**, *104*, 8632–8637.
[19] M. Levitus, G. Zepeda, H. Dang, C. Godinez, T. A. V Khuong, K. Schmieder, M. A. Garcia-Garibay, *J. Org. Chem.* **2001**, *66*, 3188–3195.
[20] a) H. Kukula, Z. M. Schops, A. Godt, *Macromolecules*, **1998**, *31*, 5160–5163; b) P. K. Tsolakis, J. K. Kallitsis, A. Godt, *Macromolecules* **2002**, *35*, 5758–5762; c) K. Li, Q. Wang, *Macromolecules* **2004**, *37*, 1172–1174; d) K. Li, Q. Wang, *Chem. Commun.* **2005**, 4786–4788.
[21] a) C. A. Breen, T. Deng, T. Breiner, E. L. Thomas, T. M. Swager, *J. Am. Chem. Soc.* **2003**, *125*, 9942–9943; b) C. A. Breen, S. Rifai, V. Bulović, T. M. Swager, *Nano. Lett.* **2005**, *5*, 1597–1601; c) C. A. Breen, J. R. Tischler, V. Bulović, T. M. Swager, *Adv. Mater.* **2005**, *17*, 1981–1985; d) K. Y. Pu, Y. Chen, X. Y. Qi, C. Y. Qin, Q. Q. Chen, H. Y. Wang, Y. Deng, Q. L. Fan, Y. Q. Huang, S. J. Liu, W. Wei, B. Peng, W. Huang, *J. Polym. Sci. Part A* **2007**, *45*, 3776–3787; e) Y. Wang, B. Erdogan, J. N. Wilson, U. H. F. Bunz, *Chem. Commun.* **2003**, 1624–1625; f) Y. Wang, J. N. Wilson, M. D. Smith, U. H. F. Bunz, *Macromolecules* **2004**, *37*, 9701–9708.
[22] S. Lu, T. X. Liu, L. Ke, D. G. Ma, S. J. Chua, W. Huang, *Macromolecules* **2005**, *38*, 8494–8502.
[23] a) K. Matyjaszewski, J. Xia, *Chem. Rev.* **2001**, *101*, 2921–2990; b) M. Kamigaito, T. Ando, M. Sawamoto, *Chem. Rev.* **2001**, *101*, 3689–3745.
[24] C. Z. Zhou, T. X. Liu, J. M. Xu, Z. K. Chen, *Macromolecules* **2003**, *36*, 1457–1464.
[25] a) C. Weder, M. S. Wrighton, *Macromolecules* **1996**, *29*, 5157–5165; b) C. Weder, M. Wrighton, R. Spreiter, C. Bosshard, P. Günter, *J. Phys. Chem.* **1996**, *100*, 18931–18936; c) U. H. F. Bunz, V. Enkelmann, L. Kloppenburg, D. Jones, K. D. Shimizu, J. B. Claridge, H. C. Z. Loye, P. Günter, *Chem. Mater.* **1999**, *11*, 1416–1424; d) P. Samorí, V. Francke, V. Enkelmann, K. Müllen, J. R. Rabe, *Chem. Mater.* **2003**, *15*, 1032–1039.
[26] a) T. Yasuda, T. Imase, Y. Nakamura, T. Yamamoto, *Macromolecules* **2005**, *38*, 4687–4697; b) H. Kokubo, T. Sato, T. Yamamoto, *Macromolecules* **2006**, *39*, 3959–3963.
[27] a) S. A. Chen, E. C. Chang, *Macromolecules* **1998**, *31*, 4899–4907; b) W. Wang, J. Xu, Y.-H. Lai, F. Wang, *Macromolecules* **2004**, *37*, 3546–3553; c) Y. Z. Lee, X. Chen, S. Chen, P. K. Wei, W. S. Fann, *J. Am. Chem. Soc.* **2001**, *123*, 2296–2307; d) S. H. Chen, C. H. Su, A. C Su, S. A. Chen, *J. Phys. Chem. B* **2004**, *108*, 8855–8861.
[28] a) Y. Pang, Q. H. Chu, *Macromolecules*, **2003**, *36*, 4614–4618; b) Q. Chu, Y. Pang, *Macromolecules* **2005**, *38*, 517–520.
[29] G. Voskerician, C. Weder, *Adv. Polym. Sci.* **2005**, *177*, 209–248.
[30] a) J. Bouchard, M. Belletête, G. Durocher, M. Leclerc, *Macromolecules* **2003**, *36*, 4624–4630; b) C. E. Halkyard, M. E. Rampey, L. Kloppenburg, S. L. Studer-Martinez, U. H. F. Bunz, *Macromolecules*, **1998**, *31*, 8655–8659.
[31] a) D. Ickenroth, S. Weissmann, N. Rumpf, H. Meier, *Eur. J. Org. Chem.* **2002**, 2808–2814; b) H. Li, D. R. Powell, T. K. Firman, R. West, *Macromolecules* **1998**, *31*, 1093–1098.
[32] a) T. Q. Nguyen, V. Doan, B. J. Schwartz, *J. Chem. Phys.* **1999**, *110*, 4068–4078; b) T. Q. Nguyen, B. J. Schwartz, *J. Chem. Phys.* **2002**, *116*, 8198–8208.
[33] a) K. Y. Peng, S. A. Chen, W. S. Fann, *J. Am. Chem. Soc.* **2001**, *123*, 11388–11397; b) S. Wang, P. Wu, Z. Han, *Macromolecules* **2003**, *36*, 4567–4576; c) Y. Chen, S. Wang, Q. Zhuang, X. Li, P. Wu, Z. Han, *Macromolecules* **2005**, *38*, 9873–9877.
[34] a) J. Kim, T. M. Swager, *Nature* **2001**, *411*, 1030–1034; b) J. Kim, I. A. Levitsky, D. T. McQuade, T. M. Swager, *J. Am. Chem. Soc.* **2002**, *124*, 7710–7718; c) S. Zahn, T. M. Swager, *Angew. Chem.* **2002**, *114*, 4399–4404; *Angew. Chem. Int. Ed.* **2002**, *41*, 4225–4230.
[35] M. I. Sluch, A. Godt, U. H. F. Bunz, M. A. Berg, *J. Am. Chem. Soc.* **2001**, *123*, 6447–6448.
[36] a) J. L. Brédas, J. Cornil, A. J. Heeger, *Adv. Mater.* **1996**, *8*, 447–451; b) K. Y. Peng, S. A. Chen, W. S. Fann, S. H. Chen, A. C. Su, *J. Phys. Chem. B* **2005**, *109*, 9368–9373.
[37] a) C. L. Chochos, P. K. Tsolakis, V. G. Gregoriou, J. K. Kallitsis, *Macromolecules* **2004**, *37*, 2502–2510; b) C. L. Chochos, J. K. Kallitcis, V. G. Gregoriou, *J. Phys. Chem. B* **2005**, *109*, 8755–8760; c) C. L. Chochos, J. K. Kallitsis, P. E. Keivanidis, S. Baluschev, V. G. Gregoriou, *J. Phys. Chem. B* **2006**, *110*, 4657–4662; d) K. T. Panagiotis, J. K. Kallitsis, *Chem. Eur. J.* **2003**, *9*, 936–943.
[38] a) A. R. Inigo, C. C. Chang, W. Fann, D. J. White, Y.-S. Huang, U.-S. Jeng, H. S. Sheu, K. Y. Peng, S. A. Chen, *Adv. Mater.* **2005**, *17*, 1835–1838; b) S. H. Chen, A. C. Su, C. S. Chang, H. L. Chen, D. L. Ho, C. S. Tsao, K. Y. Peng, S. A. Chen, *Langmuir* **2004**, *20*, 8909–8915; c) R. Jakubiak, C. J. Collison, W. C. Wan, J. Rothberg, *J. Phys. Chem. A* **1999**, *103*, 2394–2398; d) S. J. Liu, Q. Zhao, R. F. Chen, Y. Deng, Q. L. Fan, F. Y. Li, L. H. Wang, C. H. Huang, W. Huang, *Chem. Eur. J.* **2006**, *12*, 4351–4361.
[39] a) L. Leibler, *Macromolecules* **1980**, *13*, 1602–1617; b) W. Li, H. Wang, L. Yu, T. L. Morkved, H. M. Jaeger, *Macromolecules* **1999**, *32*, 3034–3044; c) B. D. Olsen, R. A. Segalman, *Macromolecules* **2005**, *38*, 10127–10137.
[40] a) J. A. Osaheni, S. A. Jenekhe, *J. Am. Chem. Soc.* **1995**, *117*, 7389–7398; b) W. Li, H. Wang, L. Yu, T. L. Morkved, H. M. Jaeger, *Macromolecules* **1999**, *32*, 3034–3944; c) X. L. Chen, S. A. Jenekhe, *Macromolecules* **2000**, *33*, 4610–4612; d) M. Lee, C.-J. Jang, J.-H. Ryu, *J. Am. Chem. Soc.* **2004**, *126*, 8082–8083; e) K. L. Genson, J. Holzmueller, M. Ornatska, Y.-S. Yoo, M.-H. Par, M. Lee, V. V. Tsukruk, *Nano Lett.* **2006**, *6*, 435–440.
[41] P. Leclère, M. Surin, P. Viville, R. Lazzaroni, A. F. M. Kilbinger, O. Henze, W. J. Feast, M. Cavallini, F. Biscarini, A. P. H. J. Schenning, E. W. Meijer, *Chem. Mater.* **2004**, *16*, 4452–4466.
[42] M. A. Horsch, Z. Zhang, S. C. Gloter, *Nano Lett.* **2006**, *6*, 2406–2413.
[43] M. Surin, D. Marsitzky, A. C. Grimsdale, K. Müllen, R. Lazzaroni, P. Leclère, *Adv. Funct. Mater.* **2004**, *14*, 708–715.
[44] P. Leclère, A. Calderone, D. Marsitzky, V. Francke, Y. Geerts, K. Müllen, J. L. Brédas, R. Lazzaroni, *Adv. Mater.* **2000**, *12*, 1042–1046.
[45] D. Neugebauer, K. Matyjaszewski, *Macromolecules* **2003**, *36*, 2598–2603.
[46] H. Shi, S. H. Chen, *Macromolecules* **1993**, *26*, 5840–5843.
[47] Q. Zhou, T. M. Swager, *J. Am. Chem. Soc.* **1995**, *117*, 12593–12602.

Received: February 23, 2007
Revised: August 27, 2007
Published online: November 14, 2007

  